Substituent Effects on Photoinitiation Ability of Coumarin-Based Oxime-Ester Photoinitiators for Free Radical Photopolymerization

Fatima Hammoud, Nicolas Giacoletto, Guillaume Noirbent, Bernadette Graff, Akram Hijazi, Malek Nechab, Didier Gigmes, Frédéric Dumur, Jacques Lalevée

Substituent Effects on Photoinitiation Ability of Coumarin-Based Oxime-Ester Photoinitiators for Free Radical Photopolymerization

Fatima Hammoud[1,2,3], Nicolas Giacoletto[4], Guillaume Noirbent[4], Bernadette Graff[1,2], Akram Hijazi[3], Malek Nechab[4], Didier Gigmes[4], Frédéric Dumur[4*] and Jacques Lalevée[1,2*]

[1] Université de Haute-Alsace, CNRS, IS2M UMR7361, F-68100 Mulhouse, France.

[2] Université de Strasbourg, France.

[3] EDST, Université Libanaise, Campus Hariri, Hadath, Beyrouth, Liban.

[4] CNRS, ICR UMR 7273, Aix Marseille Université, F-13397 Marseille, France.

Corresponding authors: Frederic.dumur@univ-amu.fr; jacques.lalevee@uha.fr

Abstract:

In this paper, a series of coumarin chromophore-based oxime-esters was designed and synthesized as visible light photoinitiators (PIs). Interestingly, upon exposure to irradiation of a LED at 405 nm, the investigated oxime-esters (OXEs) could undergo a direct photocleavage, followed by decarboxylation, generating active free radicals capable to effectively initiate acrylate polymerization. Seven of the 10 investigated OXEs have never been synthesized in the literature. Markedly, the new proposed structures exhibit also thermal initiation ability and can be used as dual photo and thermal initiators. In addition, the oxime-ester system was also paired with an iodonium salt and exhibited a higher efficiency in free radical polymerization (FRP). The chemical mechanisms and the structure/reactivity/efficiency relationships were investigated through different techniques including real-time Fourier Transform Infrared Spectroscopy (RT-FTIR), UV-visible absorption spectroscopy, fluorescence (time-resolved or steady state), cyclic voltammetry as well as molecular modelling calculations. As a proof of their remarkable polymerization performance, the new OXEs were also used at 405 nm for direct laser write applications.

Keywords: Oxime-esters, visible light, photoinitiators, dual initiators, coumarins

1. Introduction

Light-induced polymerization process has become a green chemistry technology, due to its numerous advantages such as a low energy consumption, low or no volatile organic emissions, high efficiency, and spatiotemporally controllable characteristics. [1,2] Therefore, this polymerization technique is currently widely used in the preparation of films, coatings and many other applications. [3,4] Since most of the benchmark photoinitiation systems require high-intensity UV light sources, the search for new visible light photoinitiators is a significant challenge and this topic has received an increasing attention in recent years. As visible and safe light sources, light-emitting diodes (LEDs) are an ideal alternative, as these devices are characterized by low operating costs, long lifetimes, low power consumption and these irradiation sources are now easily accessible. [5-7] Indeed, a very large number of photoinitiating systems with absorption profiles corresponding to LED emission wavelengths have been synthesized, but most of them contain more than one component, which can be complicated due to the occurrence of multiple reaction steps, hence the development of Type I (one-component) photoinitiators is now highly desirable. In this context, oxime-esters (OXEs) have long been known, as efficient Type I photoinitiators due to their reactivities in photopolymerization reactions. [8-11] Generally, their high efficiency is attributed to the direct photocleavage of the N-O bond (r1), to produce iminyl and acyloxy (R'C(=O)O$^{\bullet}$) radicals, which in turn can undergo further decarboxylation reactions. [8,12,13]

$$R_1R_2C{=}N\text{-}O\text{-}C(=O)R' \ (h\nu) \rightarrow R_1R_2C{=}N^{\bullet} + {}^{\bullet}O\text{-}C(=O)R' \rightarrow R_1R_2C{=}N^{\bullet} + CO_2 + {}^{\bullet}R' \qquad (r1)$$

The generation of CO_2 can also solve the problem of the polymerization inhibition in the presence of oxygen. [13-14] In order to shift the absorption wavelength of the oxime-esters in the visible range, recent researches have been performed e.g. by adding different chromophores to their structures, such as triphenylamine [15], phenothiazine [16], nitro-carbazole [17], or coumarin [18-19-20].

Based on other elegant studies that have specifically reported coumarin-based oxime-esters as highly efficient visible light photoinitiators, containing phenyl [18,19,20] and methoxy groups [18] as substituents, in the present paper, we studied the coumarin-based oxime-ester structural effect

on the associated photoreactivity by introducing new substituents. More particularly the huge role of the decarboxylation reaction affected by the ester group is highlighted. Interestingly, among the proposed OXEs, seven of them have never been reported in the literature and only **OXE-B**, **OXE-C** and **OXE-H** (Scheme 1) have previously been investigated. The photoinitiation ability and the photoreactivity of the proposed structures were examined upon exposure of the resins to LED@405 nm, also their thermal initiating behavior was evaluated via differential scanning calorimetry (DSC). Furthermore, and in order to highlight their high efficiency in photopolymerization, the proposed structures were used for direct laser write applications.

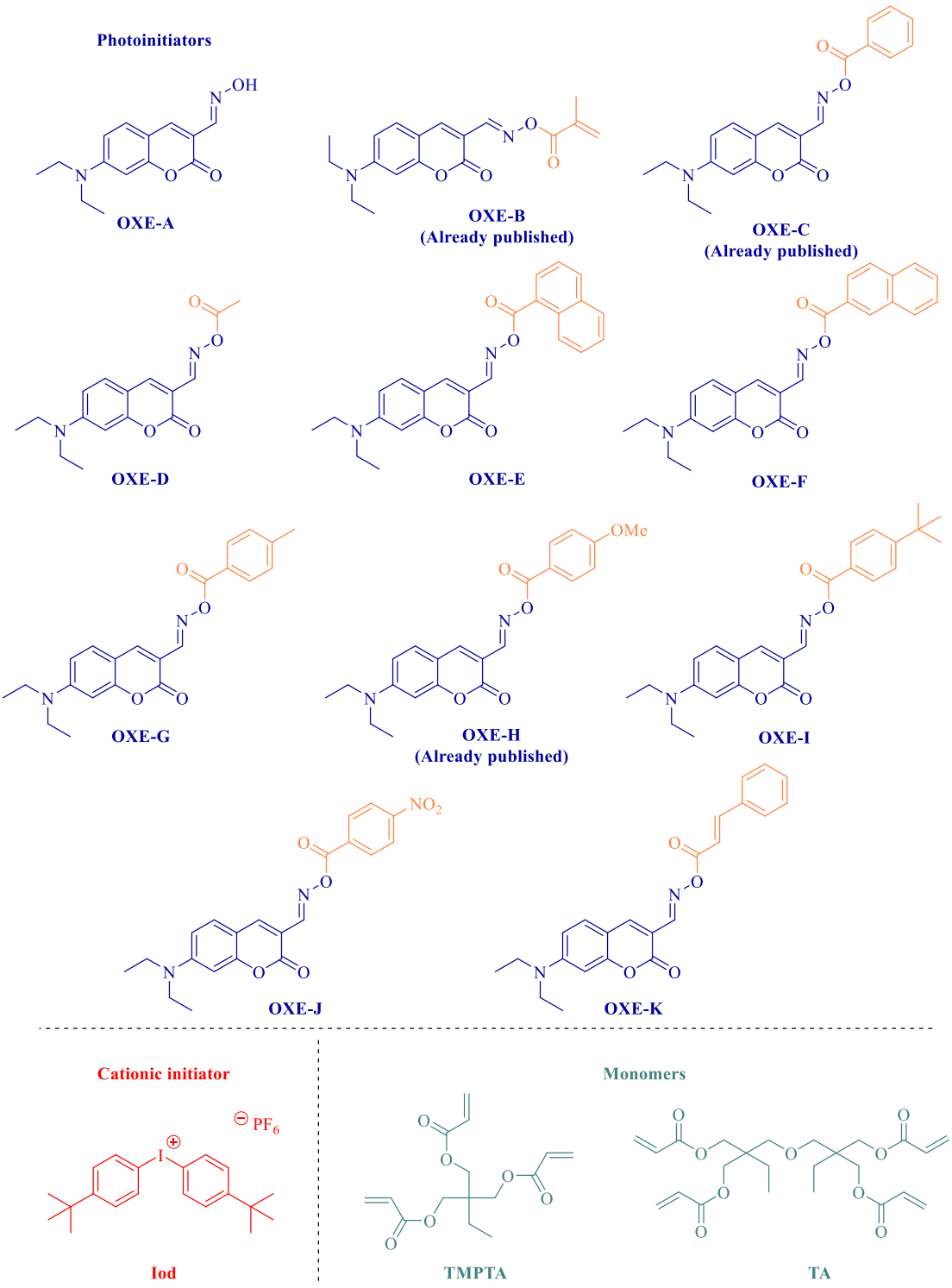

Scheme 1. Chemical structures of the synthetized coumarin-based oxime-esters, additives and monomers used in this work.

2. Experimental part

2.1. Synthesis of the investigated coumarin-based oxime-esters

Oxime **OXE-A** has been synthesized in four steps according to the procedure depicted in the Scheme 2. Starting from 4-(diethylamino)-2-hydroxybenzaldehyde (**1**) and dimethyl malonate (**2**), a coumarin with an ester function (**3**) could be obtained in 84% yield. The coumarin was then saponified and decarboxylation in acidic conditions furnished compound **4** with excellent yield (75%). By mean of a Vilsmeier Haack reaction using phosphorus oxychloride ($POCl_3$) and *N*,*N*-dimethylformamide, an aldehyde function could be introduced onto **4**, providing **5** in 89% yield. By reaction with hydroxylamine hydrochloride and sodium acetate in a mixture of solvent (THF, MeOH, H_2O), the oxime **OXE-A** could be obtained in 92% yield. Then, the oxime was esterified with different acid chlorides to provide ten oxime-esters (**OXE-B – OXE-K**) as described in the Scheme 2. Structural modification of the acid chlorides consisting in using aliphatic acid chlorides, aromatic acid chlorides or an acid chloride bearing a crosslinkable function were used to investigate the reactivity of the different radicals formed. Detailed synthetic procedures and structural characterizations for each oxime-ester are presented in the ESI. Most of the oxime-esters could be obtained in pure form by mean of a simple precipitation in diethyl ether. However, several oxime-esters also required to be purified by chromatography column (SiO_2). The different oxime-esters could be obtained with reaction yields ranging from 51% to 91%. It has to be noticed that for **OXE-B,** the reaction yield was lower compared to that of the other oxime-esters due to a partial polymerization of the methacrylate function during the purification process but also during the removal of the solvent by rotary evaporation, evidencing the high reactivity of this functional group.

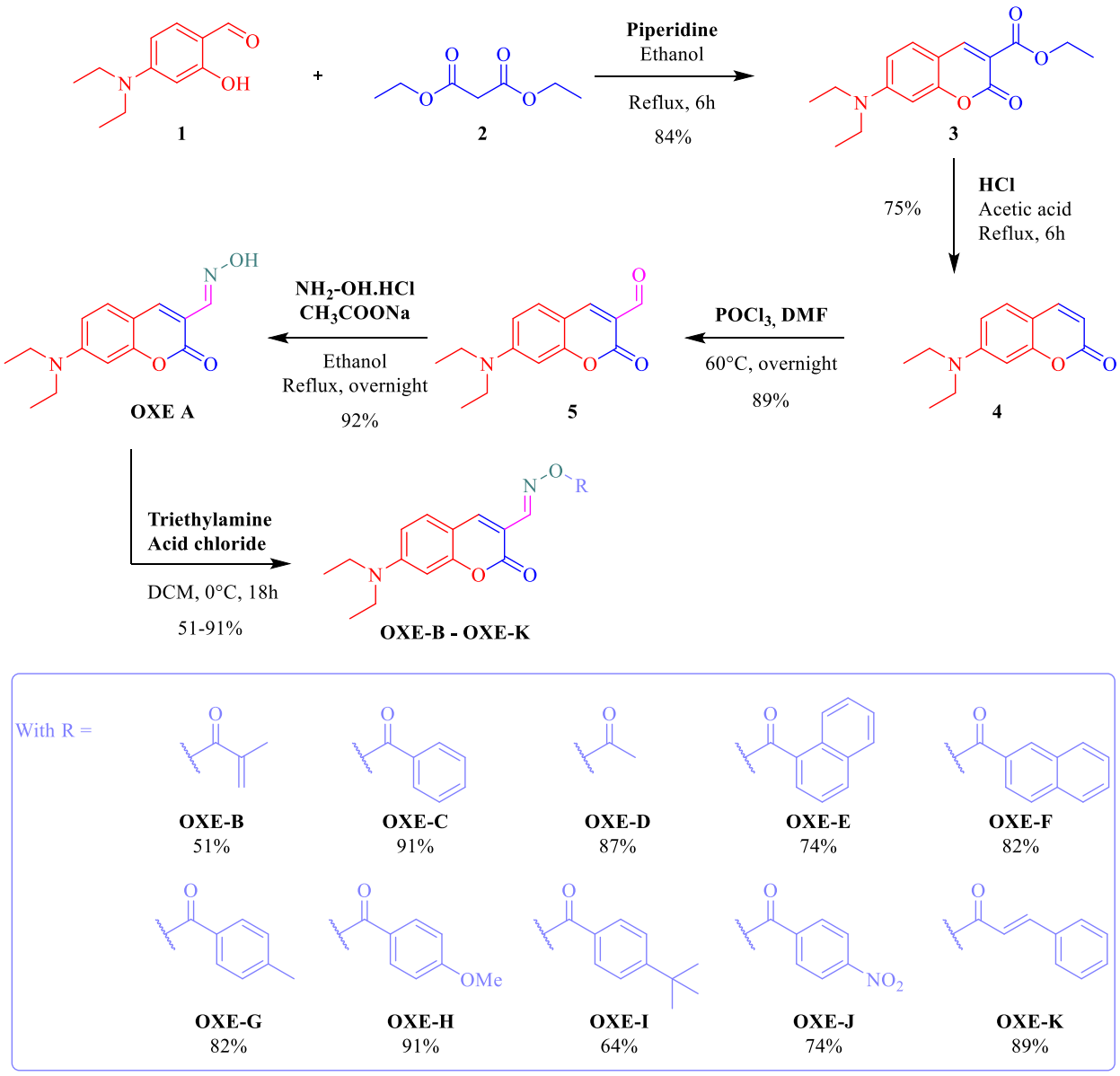

Scheme 2. Synthetic routes to OXE-A – OXE-K.

2.2. Other Chemicals compounds

Bis-(4-*tert*-butylphenyl)iodonium hexafluorophosphate (Iod; SpeedCure 938) was obtained from Lambson Ltd (UK). The monomers were obtained from Allnex. Chemical structures of monomers and additives are shown in Scheme 1.

2.3. Irradiation Source

The following light emitting diode (LED) was used as irradiation source: LED @405 nm with an incident light intensity at the sample surface: $I_0 = 110$ mW.cm^{-2}.

2.4. UV-visible absorption and photolysis experiments

The UV-visible absorption properties of the different compounds as well as the steady state photolysis were studied using a JASCO V730 UV-visible spectrophotometer.

2.5. Photopolymerization kinetics (RT-FTIR)

The experimental conditions for each photosensitive formulation are indicated in the caption of the figures. All the polymerizations were performed at room temperature and the irradiation was started after t = 10 s. The weight of the photoinitiating system is calculated from the monomer content. The conversions of the acrylate functions of the TMPTA or TA were continuously followed by real time FTIR (RT-FTIR) spectroscopy (JASCO FTIR 4100). The photopolymerization experiments were carried out in laminate (the formulation is sandwiched between two polypropylene films to reduce the O_2 inhibition). The decrease of C=C double bond peak was continuously monitored from 1581 to 1662 cm^{-1}. The procedures were described by us in references [21-22].

2.6. Computational procedure

Molecular orbital calculations were carried out using the Gaussian 03 suite of programs. The electronic absorption spectra for the different compounds were calculated with time-dependent density functional theory at the MPW1PW91/6-31G* level of theory on the relaxed geometries calculated at the UB3LYP/6-31G* level of theory. The triplet state energy levels were calculated at this level of theory after full optimization of the excited state.

2.7. Fluorescence experiment

Steady state fluorescence. Fluorescence spectra were acquired in a quartz cell at room temperature using a JASCO FP-750 spectrofluorometer.

Time correlated single photon counting (TCSPC). The fluorescence excited state lifetimes were determined using a time correlated single-photon counting system, a HORIBA DeltaFlex with a HORIBA PPD-850 as detector. The excitation source is a HORIBA nanoLED-370 with an excitation wavelength of 367 nm and a pulse duration inferior to 1.4 ns. The fluorescence intensity decay profiles were recorded in acetonitrile in a quartz cell. A silica colloidal solution LUDOX was used to evaluate the impulse response function (IRF) of the apparatus.

2.8. Redox potentials

The redox potentials (E_{ox} and E_{red}) were measured in acetonitrile by cyclic voltammetry using tetrabutylammonium hexafluorophosphate (0.1 M) as the supporting electrolyte (potential vs. Saturated Calomel Electrode – SCE). The free energy change ΔG_{et} for an electron transfer reaction was calculated from eqn (1), [23] where E_{ox}, E_{red}, E*, and C are the oxidation potential of the electron donor, the reduction potential of the electron acceptor, the excited state energy and the coulombic term for the initially formed ion pair, respectively. Here, C is neglected for polar solvents.

$$\Delta G_{et} = E_{ox} - E_{red} - E^* + C \qquad \text{(Eqn. 1)}$$

2.9. Differential Scanning Calorimetry (DSC) For Thermal Polymerization

About 10 mg of TMPTA containing 1% w oxime-ester initiator (OXE) was inserted into a 100 µL aluminum crucible. Thermal polymerization was performed from room temperature to 300 °C at a heating rate of 10 °C/min. under nitrogen flow (100 mL/min.). A Mettler Toledo DSC 1 differential scanning calorimeter was used.

2.10. Direct Laser Write

For direct laser write experiments, a laser diode @405 nm (spot size around 50 µm) was used for the spatially controlled irradiation. The photosensitive resin was polymerized under air

and the generated 3D patterns were analyzed using a numerical optical microscope (DSX-HRSU from Olympus Corporation) as presented in the references [24-28].

3. Results and discussion

3.1. UV-visible absorption

The UV-visible absorption spectra of the new proposed oxime-ester derivatives in acetonitrile are shown in Figure 1. Their maximum absorption wavelengths (λ_{max}), extinction coefficients (ε_{max}) at λ_{max} and at the emission wavelength @405 nm are also gathered in Table 1.

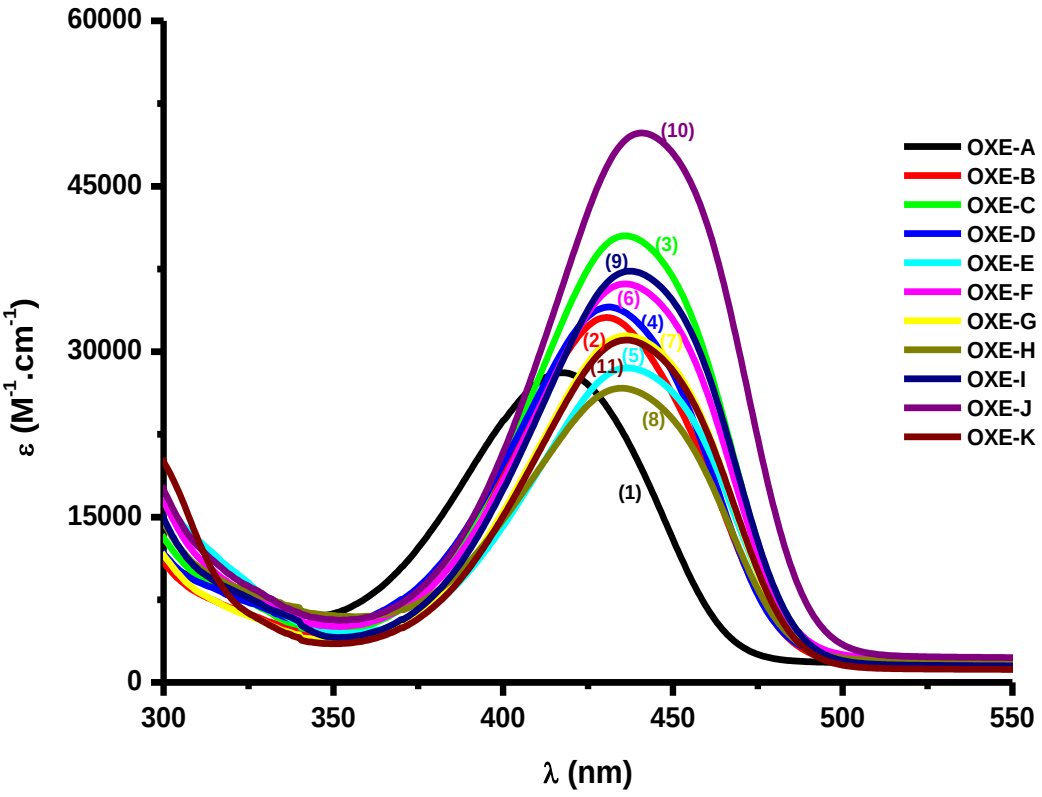

Figure 1. UV-visible absorption spectra of the investigated coumarin-based oxime-esters in acetonitrile: (1) OXE-A; (2) OXE-B; (3) OXE-C; (4) OXE-D; (5) OXE-E; (6) OXE-F; (7) OXE-G; (8) OXE-H; (9) OXE-I; (10) OXE-J; and (11) OXE-K.

Table 1. Light absorption properties of the investigated compounds; maximum absorption wavelengths (λ_{max}), extinction coefficients at λ_{max} and extinction coefficients at @405 nm.

PI	λ_{max} (nm)	ε_{max} ($M^{-1}.cm^{-1}$)	$\varepsilon_{(405nm)}$ ($M^{-1}.cm^{-1}$)
OXE-A	418	28000	25500
OXE-B	431	33000	22000
OXE-C	436	40500	23500
OXE-D	431	34000	22500
OXE-E	437	28500	16500
OXE-F	437	36000	21000
OXE-G	436	31500	18000
OXE-H	435	26500	17000
OXE-I	437	37000	20500
OXE-J	441	50000	25000
OXE-K	435	31000	18000

The maximum absorption wavelength (λ_{max}) of **OXE-A** is located at 418 nm. Upon introduction of the oxime-ester functionality, the λ_{max} of OXEs is slightly redshifted compared to that of **OXE-A**. All the new investigated oxime-esters exhibit high molar extinction coefficients (e.g. **OXE-C** ε ~ 40500 $M^{-1}.cm^{-1}$ at 436 nm and 23500 $M^{-1}.cm^{-1}$ at 405 nm, and **OXE-J** ε ~ 50000 $M^{-1}.cm^{-1}$ at 441 nm and ~ 25000 $M^{-1}.cm^{-1}$ at 405 nm). Therefore, absorption properties of the different dyes allow a good overlap with the emission spectra of the visible LED used in this work.

3.2. Type I initiator behavior

For the polymerization of TMPTA-acrylate monomer, the photoinitiation abilities of OXEs (0.5% w) as Type I photoinitiators were studied using RT-FTIR in thin films upon irradiation with LED@405 nm at room temperature. Typical final acrylate function conversions (FCs) vs.

irradiation time profiles are given in Figure 2. The associated final FCs and the polymerization rates are summarized in Table 2.

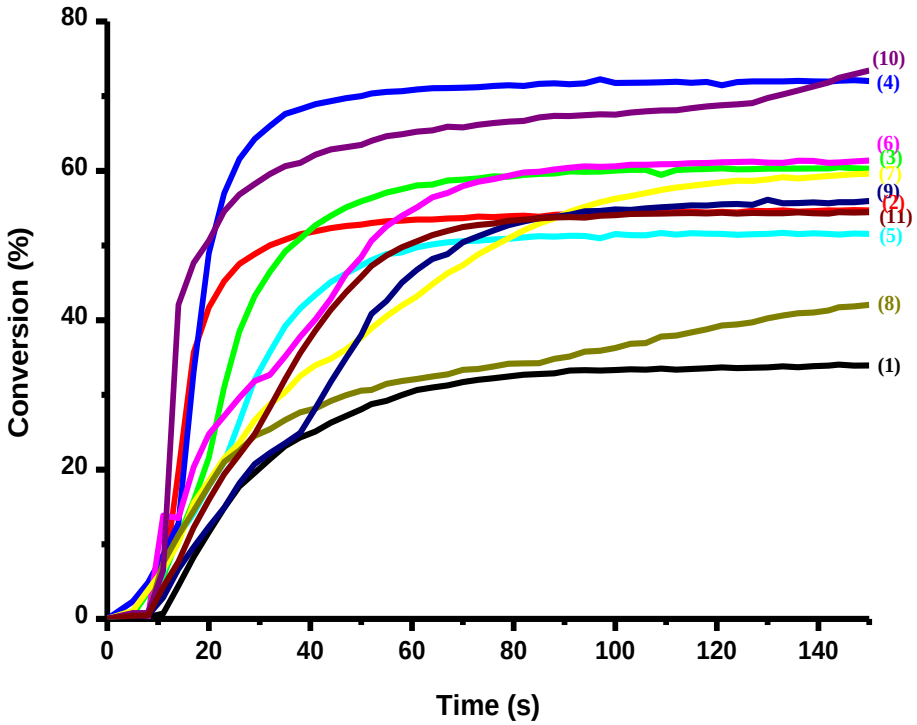

Figure 2. Photopolymerization profiles of TMPTA (acrylate function conversion vs. irradiation time) in laminate (thickness = 25 µm) upon exposure to LED light λ = 405 nm in the presence of: (1) OXE-A (0.5% w); (2) OXE-B (0.5% w); (3) OXE-C (0.5% w); (4) OXE-D (0.5% w); (5) OXE-E (0.5% w); (6) OXE-F (0.5% w); (7) OXE-G (0.5% w); (8) OXE-H (0.5% w); (9) OXE-I (0.5% w); (10) OXE-J (0.5% w); and (11) OXE-K (0.5% w); respectively. The irradiation starts after t = 10 s.

Table 2. Final acrylate function conversion (FCs) and the polymerization rate for TMPTA using one component (1% w) photoinitiators after irradiation with LED light (λ= 405 nm).

PI	Final Conversion (FC) (%)	$R_p/[M]_0$ x 100 (s^{-1}) (after t= 10 s)
OXE-A	34	1.14
OXE-B	55	5.17
OXE-C	60	1.16
OXE-D	72	6.03
OXE-E	52	1.22
OXE-F	61	2.39
OXE-G	59	1.58
OXE-H	42	1.05
OXE-I	56	0.99
OXE-J	73	5.61
OXE-K	54	1.09

OXE-A (without the oxime-ester function) has a very low photoinitiation ability in comparison with the other OXEs, which clearly highlights the importance of the oxime-ester function to act as a Type I photoinitiator. **OXE-J** reaches the highest final conversion of 73%, which can be attributed to its highest absorption properties ($\varepsilon_{max\ (OXE\text{-}J)}$= 50000 $M^{-1}.cm^{-1}$), and **OXE-D** also achieves a final conversion of 72%, which is higher than other OXEs that have higher absorption abilities (see Figure 1 and Table 1). Furthermore, it is clearly noticed that the polymerization rates are not the same and the difference between them is not directly related to the absorption properties, hence the importance of introducing other factors that can also play an important role in the photopolymerization process such as the cleavage reaction, the decarboxylation reaction as well as the reactivity of the generated radicals.

Table 3. Parameters characterizing the investigated OXEs. Some parameters characterizing the proposed oxime-esters were calculated by molecular modelling: the Bond Dissociation Energy BDE (N-O), the triplet state energy E_{T1}, the enthalpy $\Delta H_{cleavageT1}$ for cleavage process from T_1, the enthalpy $\Delta H_{decarboxylation}$ for decarboxylation reaction and the spin density. The singlet excited state energy E_{S1}, the enthalpy $\Delta H_{cleavageS1}$ for cleavage process from S_1, and the fluorescence lifetime of the OXEs were measured experimentally.

PI	BDE (N-O) (kcal.mol^{-1})	E_{S1} (kcal.mol^{-1})	$\Delta H_{cleavage\ S1}$ (kcal.mol^{-1})	τ_0 (S1) (ns)	E_{T1} (kcal.mol^{-1})	$\Delta H_{cleavage\ T1}$ (kcal.mol^{-1})	$\Delta H_{decarboxylation}$ (kcal.mol^{-1})	Spin density ($R^{\bullet}$)
OXE-A	64.56	61.8	2.76	3.36	42.70	21.86	-	-
OXE-B	42.31	59.72	-17.41	1.92	47.49	-5.18	0.52	0.999
OXE-C	48.42	59.26	-10.84	1.65	44.67	3.75	5.92	0.989
OXE-D	48.87	60.42	-11.55	1.89	44.83	4.04	-4.94	1.156
OXE-E	45.54	59.49	-13.95	1.64	44.74	0.8	4.36	0.999
OXE-F	48.34	59.26	-10.92	1.61	44.60	3.74	6.24	0.995
OXE-G	48.14	59.03	-10.89	1.65	44.61	3.53	6.92	0.990
OXE-H	47.85	58.57	-10.72	1.79	44.51	3.34	8.77	0.996
OXE-I	48.13	59.49	-11.36	1.58	44.61	3.52	6.97	0.989
OXE-J	50.58	-	-	-	44.78	5.8	3.14	0.998
OXE-K	49.09	59.72	-10.63	0.989	44.42	4.67	7.64	1.076

Fluorescence lifetime of OXEs was also measured (Table 3, Figure 3 (B)). **OXE-A** has the longest lifetime (3.36 ns), which is significantly reduced after the introduction of the oxime-ester function suggesting a cleavage from S_1 in full agreement with an energetically favorable process from S_1 ($\Delta H_{cleavage\ S1}$= BDE (N-O) – E_{S1}) (see Table 3). The singlet excited state energy levels (E_{S1}) were determined from the crossing point of absorption and fluorescence spectra (Figure 3 (A)). The triplet state energy (E_T) and the N-O bond energy of the investigated OXEs were calculated (Table 3). Markedly, the N-O bond dissociation energy for all OXEs (expect **OXE-B**)

are higher than their calculated triplet state energy levels (see Table 3) i.e. cleavages from T_1 are not energetically favorable ($\Delta H_{cleavage\ T1}$= BDE (N-O) – E_{T1} > 0) – excepted for **OXE-B** (Table 3).

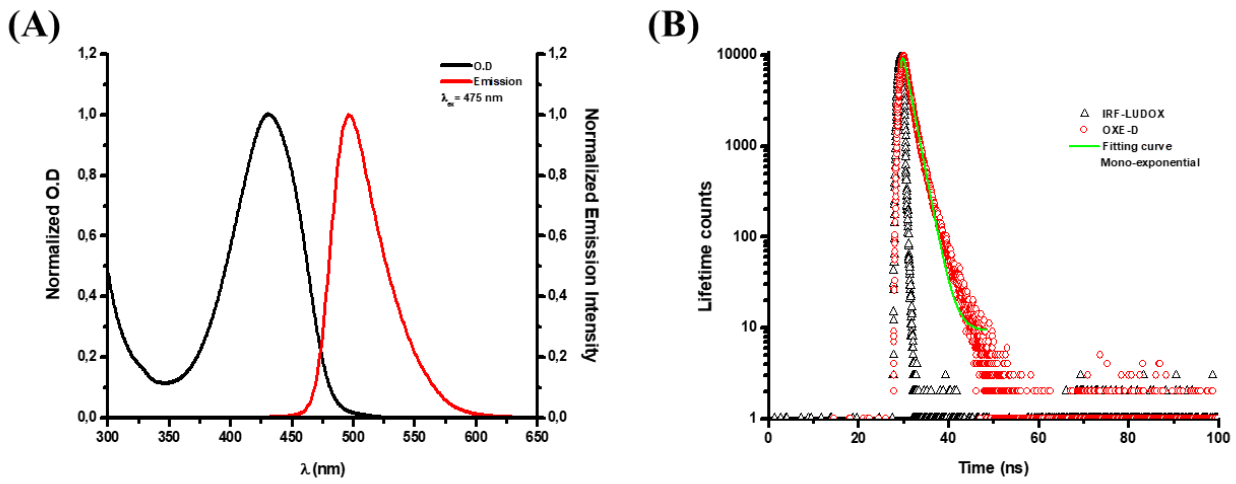

Figure 3. (A) UV-visible absorption and emission spectra of **OXE-D** in acetonitrile. (B) Time correlated single-photon counting of **OXE-D** in acetonitrile, λ_{ex}= 367 nm, λ_{em}= 450 nm, mono-exponential curve fitting.

In order to study the photolysis behavior after light irradiation, the steady state photolysis was carried out in acetonitrile for the different OXEs, at room temperature with different irradiation time. The change in the intensity of the absorption band indicates the clear occurrence of photoreactions. For example, for **OXE-D** (Figure 4(A)) after 5 minutes of irradiation, the maximum peak is slightly shifted to shorter wavelength and the absorbance increased.

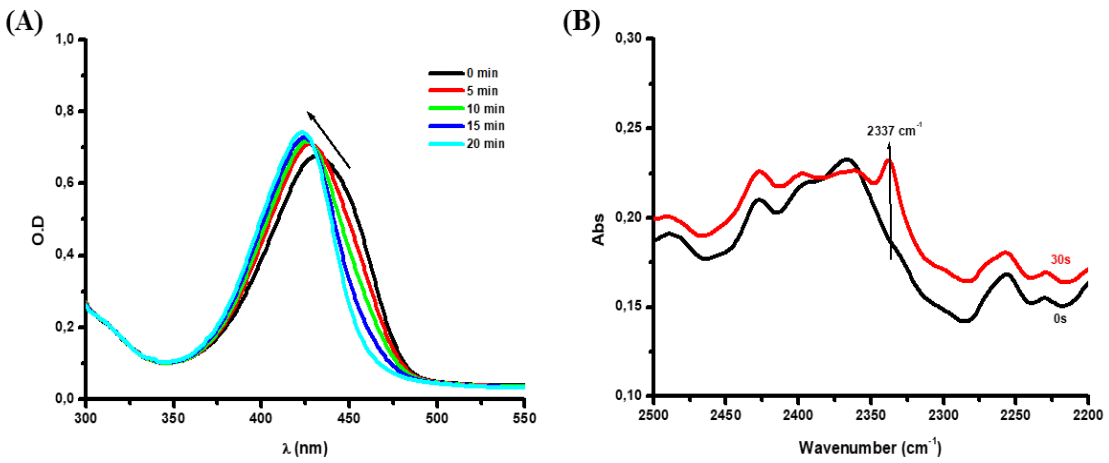

Figure 4. (A) Steady state photolysis of **OXE-D** upon LED@375 nm in acetonitrile; (B) The detection of CO_2 for **OXE-D** system.

OXEs have been reported to undergo photoinduced decarboxylation in high quantum yields. [28-29] Remarkably, as we can see from Table 3, we can notice that the decarboxylation reaction is energetically the most favorable in the case of **OXE-D** ($\Delta H_{decarboxylation} = E_{(R\bullet)} + E_{(CO2)} - E_{(RC(=O)O\bullet)}$ = -4.94 kcal.mol^{-1} – Table 3), the generated CO_2 was detected by real time Fourier transformed infrared spectroscopy (RT-FTIR) and the infrared spectra of **OXE-D** at t = 0 s and t = 30 s are presented in Figure 4(B). For the other OXEs, this peak is not observed suggesting a low decarboxylation yield in agreement with an unfavorable process ($\Delta H_{decarboxylation} > 0$; Table 3). Furthermore, the radicals produced ($R^{\bullet}$) must be efficient for an initiation reaction (addition on a C=C double bond). This parameter was evaluated by looking at the spin density on the radical center ($C^{\bullet}$ radicals in our case). In a first approach, the more localized is the spin, the more reactive (less stabilized by delocalization) the free radical will be [3]. **OXE-D** has the highest spin density (1.156), i.e. leading to reactive methyl radicals. This can explain the high reactivity of **OXE-D** in the photopolymerization process compared to the other OXEs as the decarboxylation is much less favorable for the other OXEs.

Besides the photoinitiation behavior, thermal initiating abilities of the oxime-esters were also studied by DSC in the dark, both the maximum and onset temperatures are given in Table 4. Markedly, **OXE-D** is found both as an excellent thermal and photochemical initiator, as it initiates polymerization at a lower temperature 155°C (Table 4) than the other OXEs.

Table 4. Maximal polymerization temperatures for TMPTA using OXE (1% w) as thermal initiators under N_2.

PI	OXE-B	OXE-C	OXE-D	OXE-E	OXE-F	OXE-G	OXE-H	OXE-I	OXE-J	OXE-K
T_{max} (°C)	209	215	181	205	208	207	212	212	215	210
T_{onset} (°C)	170	186	155	171	169	166	180	186	198	173

3.3. Two-component initiator behavior

The photoinduced free radical photopolymerization of TMPTA acrylate monomer in the presence of OXE/Iod (0.5%/1% w/w) was also investigated upon the LED at 405 nm. The typical double bond conversion profiles are presented in Figure 5 and the associated final acrylate function conversions (FCs) are summarized in Table 5.

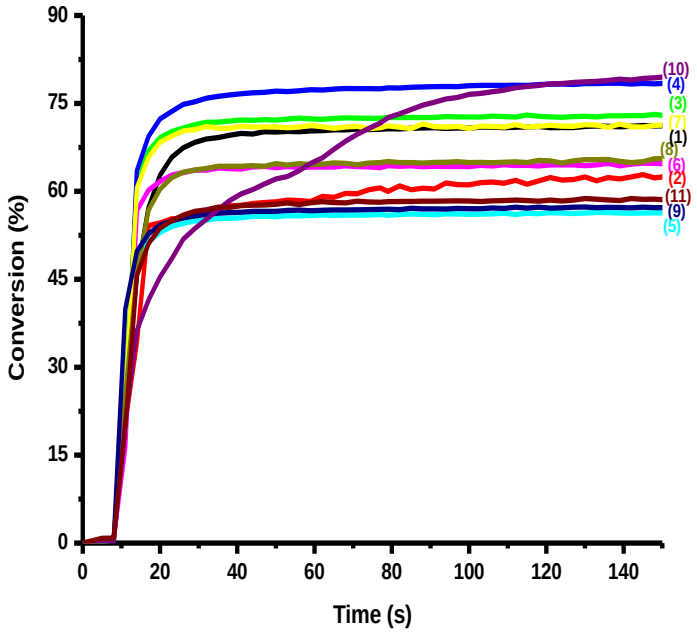

Figure 5. Photopolymerization profiles of TMPTA (acrylate function conversion vs. irradiation time) in laminate (thickness= 25 µm) upon exposure to LED light λ= 405 nm in the presence of: (1) **OXE-A**/Iod (0.5%/1% w/w); (2) **OXE-B**/Iod (0.5%/1% w/w); (3) **OXE-C**/Iod (0.5%/1% w/w); (4) **OXE-D**/Iod (0.5%/1% w/w); (5) **OXE-E**/Iod (0.5%/1% w/w); (6) **OXE-F**/Iod (0.5%/1% w/w); (7) **OXE-G**/Iod (0.5%/1% w/w); (8) **OXE-H**/Iod (0.5%/1% w/w); (9) **OXE-I**/Iod (0.5%/1% w/w); (10) **OXE-J**/Iod (0.5%/1% w/w); and (11) **OXE-K**/Iod (0.5%/1% w/w); respectively. The irradiation starts for t = 10 s.

Table 5. Final acrylate function conversion (FCs) for TMPTA using OXE/Iod (0.5%/1% w/w) as photoinitiating systems after 100 s of irradiation with LED light (λ= 405 nm) in laminate.

PI	OXE-A	OXE-B	OXE-C	OXE-D	OXE-E	OXE-F	OXE-G	OXE-H	OXE-I	OXE-J	OXE-K
Final acrylate function Conversion (FC) (%)	71	63	73	78	56	65	71	66	57	79	59

The experimental results show that the OXEs/Iod systems have faster polymerization rates and higher final conversions compared to those achieved with OXEs alone without Iod (Figure 2 vs. Figure 5). The trend of the final acrylate function conversion efficiency of the OXEs in the two-component system in thin samples (25 µm, in laminate) is **OXE-J** ~ **OXE-D** > **OXE-C** > **OXE-A** ~ **OXE-G** > **OXE-H** > **OXE-F** > **OXE-B** > **OXE-K** > **OXE-I** > **OXE-E**, which is not directly related to the absorption properties of the studied oxime-esters ($\varepsilon_{405\ nm}$), but also to their photochemical reactivity with the iodonium salt which is probably affected by the structure of the OXE and also probably by the yield of electron transfer with Iod to generate initiating aryl radicals (see below (r2-r3)).

In order to better understand the interaction between the coumarin-based oxime-esters and the iodonium salt (Iod), fluorescence quenching experiments were carried out. Interestingly, a strong fluorescence quenching processes of ^{1}**OXE** by Iod was detected (see Figure 6 and Table 6); this clearly shows a very strong interaction of ^{1}**OXE** with Iod (r2-r3). The oxidation potentials (E_{ox}) determined by cyclic voltammetry (Table 6) allow the evaluation of the free energy change (ΔG) for these electron transfer reactions (Table 6). Markedly, highly favorable ΔG are found in agreement with these strong ^{1}**OXE-A**/Iod interactions (i.e. fluorescence quenching). The associated electron transfer quantum yields (Φ_{et}) were determined according to the following equation: $\Phi_{et} = k_{sv}[Iod]/(1+k_{sv}[Iod])$ and high Φ_{et} are found (e.g., Φ= 0.72 for **OXE-A**, Table 6).

$$OXE\ (h\nu) \rightarrow {}^1OXE \qquad (r2)$$

$$^1OXE + Ar_2I^+ \rightarrow OXE^{\bullet+} + Ar^{\bullet} + ArI \qquad (r3)$$

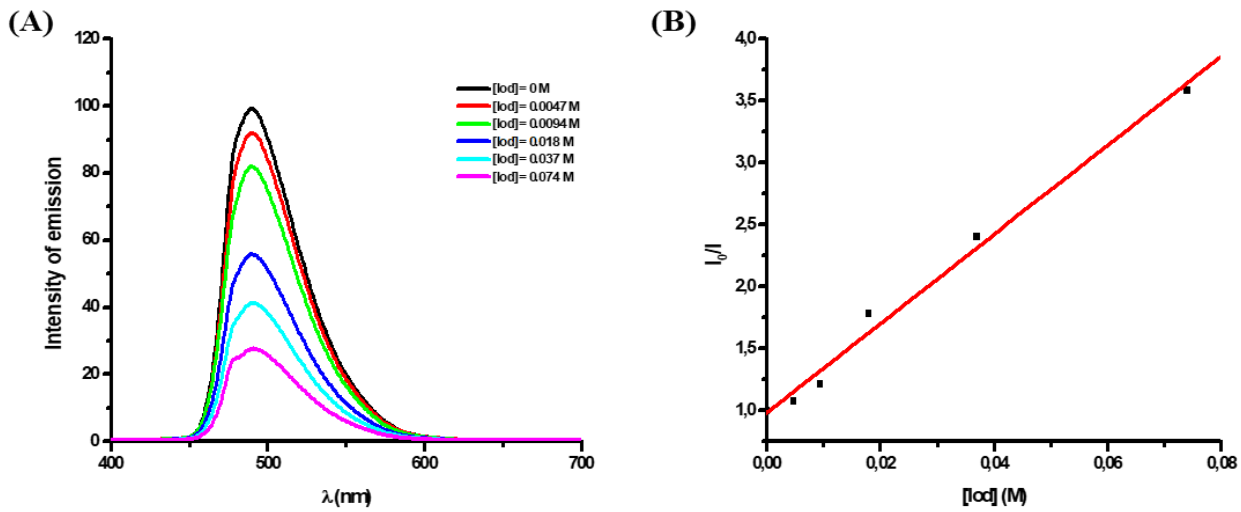

Figure 6. (A) Quenching of ^{1}**OXE-A** by Iod in acetonitrile. (B) Representation of the associated Stern-Volmer plot.

Table 6. Parameters characterizing the chemical mechanisms associated with the oxime-esters/Iod interaction in acetonitrile.

PI	E_{ox} (ev)	E_{S1} (ev)	$\Delta G_{S1\ (Iod)}$ (eV)[a]	K_{sv} (M^{-1})[b]	$\Phi_{et(OXE/Iod)}$
OXE-A	0.98	2.68	-1.00	36	0.72
OXE-B	1.03	2.59	-0.86	23	0.61
OXE-C	1.11	2.57	-0.76	17	0.51
OXE-D	1.06	2.62	-0.86	27	0.66
OXE-E	1.05	2.58	-0.83	23	0.61
OXE-F	1.05	2.57	-0.82	18	0.55
OXE-G	1.04	2.56	-0.82	38	0.71
OXE-H	1.06	2.54	-0.82	56	0.78
OXE-I	1.05	2.58	-0.83	16	0.53
OXE-J	1.06	-	-	-	-
OXE-K	1.04	2.59	-0.85	11	0.43

a: evaluated from $\Delta G_{S1} = E_{ox} - E_{red}(Iod) - E_{S1}$; $E_{red}(Iod)$ = -0.7 V from [22].

b: Stern-Volmer coefficient (K_{sv}); slope of the quenching curve: $I/I_0=(1+ksv[Iod])$.

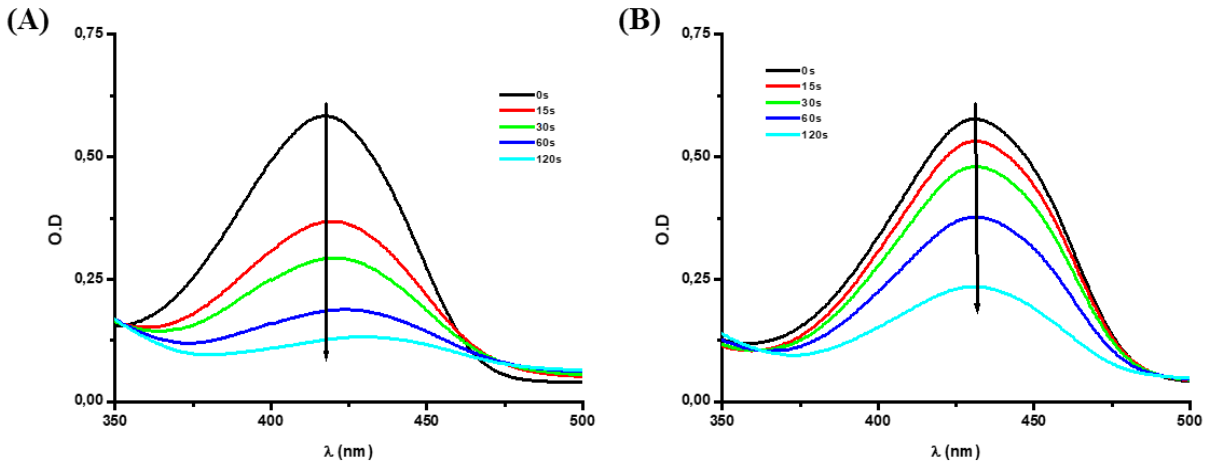

Figure 7. (A) Photolysis of **OXE-A** with Iod (10^{-2} M) in acetonitrile; (B) photolysis of **OXE-D** with Iod (10^{-2} M) in acetonitrile.

The steady state photolysis of OXEs/Iod (10^{-2} M) is carried out in acetonitrile upon irradiation light using a LED@375 nm. This photolysis is much faster with Iod (Figure 7) than without Iod (Figure 4) showing that the direct cleavage of OXEs is less favorable than their interaction with iodonium in their first excited singlet state. This strong ^{1}OXE/Iod interaction is in full agreement with the results observed in the photopolymerization experiments.

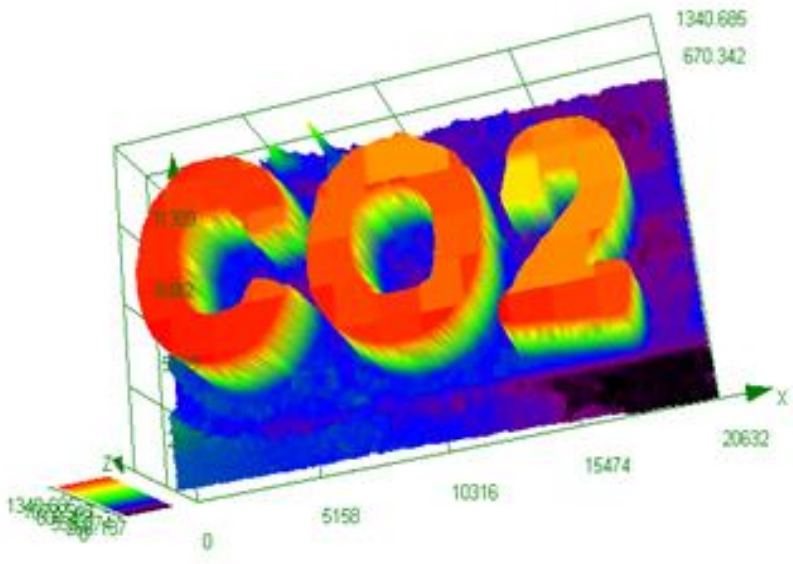

Figure 8. Optical microscopy of the 3D patterns obtained from **OXE-D**/Iod (0.1%/1% w/w) in a TA, upon exposure to a laser diode @405 nm.

3D printing experiment upon light irradiation at 405 nm using the two-component photoinitiating system, **OXE-D**/Iod (0.1%/1% w/w) in TA was successfully performed under air. Indeed, the high photosensibility of this system allows an efficient polymerization in the irradiated area. 3D patterns elaborated with high spatial resolution and very short writing time (~2 min.), were characterized by numerical optical microscopy (Figure 8).

4. Conclusion

In this article, ten structures of coumarin-based oxime-esters varying by the ester group substitution were successfully synthetized. Interestingly, among the proposed OXEs, seven of them have never been reported in the literature and only **OXE-B**, **OXE-C** and **OXE-H** have previously been synthesized. Their performances in the free radical polymerization were examined under light irradiation using a LED@405 nm. Some relevant structure/efficiency relationships were discussed based on their light absorption properties, cleavage ability, decarboxylation reaction as well as reactivity of the generated radicals. The methyl group in **OXE-D** leads to the most favorable decarboxylation process that is the key point for the formation of efficient carbon centered radicals. In addition, the thermal initiator feature was evaluated, in order to show their dual thermal/photochemical initiator behavior. Again, **OXE-D** is characterized by the most favorable behavior. This work opens a new direction for the development of redshifted OXEs to make them applicable to longer wavelength and shows the importance of the thermal initiator ability as a complement for polymerization in shadow areas where a thermal process can overcome the light penetration issue. Other dual-cure systems (thermal/photochemical) will be proposed in forthcoming studies to overcome the issue of shadow areas.

References

[1] C. Dietlin, S. Schweizer, P. Xiao, J. Zhang, F. Morlet-Savary, B. Graff, J. P Fouassier, J. Lalevée, Photopolymerization upon LEDs: new photoinitiating systems and strategies. Polymer Chemistry, 2015, 6.21: 3895-3912.

[2] P. Garra, C. Dietlin, F. Morlet-Savary, F. Dumur, D. Gigmes, J.P. Fouassier, J. Lalevée, Photopolymerization processes of thick films and in shadow areas: a review for the access to composites. Polymer Chemistry, 2017, *8*.46: 7088-7101.

[3] C. Dietlin, T.T. Trinh, S. Schweitzer, B. Graff, F. Morlet-Savary, P.A. Noirot, J. Lalevée, Rational Design of Acyldiphenylphosphine Oxides as Photoinitiators of Radical Polymerization. Macromolecules, 2019, 52**:** 7886-7893.

[4] F. Karasu, C. Croutxé-Barghon, X. Allonas, D. V. Van, G. J. Leendert, Free radical photopolymerization initiated by UV and LED: Towards UV stabilized, tack free coating. J Polym Sci, Part A: Polym Chem, 2015, 52.24: 3597-607.

[5] J. Kirschner, J. Paillard, M. Bouzrati-Zerelli, J.M. Becht, JE Klee, S. Chelli, S. Lakhdar, J. Lalevée, Aryliodonium Ylides as Novel and Efficient Additives for Radical Chemistry: Example in Camphorquinone (CQ)/Amine Based Photoinitiating Systems. Molecules, 2019, 24: 2913-2923.

[6] N. Zivic, M. Bouzrati, S. Villote, F. Morlet-Savary, C. Dietlin, F. Dumur, D. Gigmes, J.P. Fouassier, J. Lalevée, A novel naphthalimide scaffold based iodonium salt as a one-component photoacid/photoinitiator for cationic and radical polymerization under LED exposure. Polymer Chemistry, 2016, 7: 5873-5879.

[7] M. Topa, E. Hola, M. Galek, F. Petko, M. Pilch, R. Popielarz, F. Morlet-Savary, B. Graff, J. Lalevée, J. Ortyl, One-component cationic photoinitiators based on coumarin scaffold iodonium salts as highly sensitive photoacid generators for 3D printing IPN photopolymers under visible LED sources. Polymer Chemistry, 2020, 11: 5261–5278.

[8] Y. Pang, S. Fan, Q. Wang, D. Oprych, A. Feilen, K. Reiner, D. Keil, Y. Slominsky, S. Popov, Y. Zou, B. Strehmel, NIR-Sensitized Activated Photoreaction between Cyanines and Oxime Esters: Free-Radical Photopolymerization. Angewandte Chemie International Edition, 2020, 59.28: 11440-11447.

[9] S. Chen, M. Jin, J.P. Malval, J. Fu, F. Morlet-Savary, H. Pan, D. Wan, Substituted stilbene-based oxime esters used as highly reactive wavelength-dependent photoinitiators for LED photopolymerization. Polymer Chemistry, 2019, 10.48: 6609-6621.

[10] J. Xu, G. Ma, K. Wang, J. Gu, S. Jiang, J. Nie, Synthesis and photopolymerization kinetics of oxime ester photoinitiators. Journal of Applied Polymer Science, 2012, 123.2: 725-731.

[11] R. Zhou, X. Sun, R. Mhanna, J. P. Malval, M. Jin, H. Pan, D. Wan, F. Morlet-Savary, H. Chaumeil, and C. Joyeux, Wavelength-Dependent, Large-Amplitude Photoinitiating Reactivity within a Carbazole-Coumarin Fused Oxime Esters, Series. ACS Applied Polymer Materials, 2020, 2.5: 2077-2085.

[12] W. Wang, M. Jin, H. Pan and D. Wan, Phenylthioether thiophene-based oxime esters as novel photoinitiators for free radical photopolymerization under LED irradiation wavelength exposure. Progress in Organic Coatings, 2021, 151, 106019.

[13] X. Y. Ma, D. Cao, H. Y. Fu, J. You, R. Q. Gu, B. F. Fan, J. Nie and T. Wang, Multicomponent photoinitiating systems containing arylamino oxime ester for visible light photopolymerization, Progress in Organic Coatings, 2019, 135, 517-524.

[14] W. Wang, M. Jin, H. Pan, D. Wan, Remote Effect of Substituents on the Properties of Phenyl Thienyl Thioether-based Oxime Esters as LED-sensitive Photoinitiators. Dyes and Pigments, 2021, 109435.

[15] Z.H. Kee, F. Hammoud, A. Hijazi, B. Graff, J. Lalevée, YC Chen, Synthesis and free radical photopolymerization of triphenylamine-based oxime ester photoinitiators. Polymer Chemistry, 2021, 12**:** 1286-1297.

[16] X. Y. Ma, R. Q. Gu, L. J. Yu, W. X. Han, J. Li, X. Y. Li, T. Wang, Conjugated phenothiazine oxime esters as free radical photoinitiators. Polymer Chemistry, 2017, 8, 6134-6142.

[17] S. Liu, B. Graff, P. Xiao, F. Dumur, J. Lalevée, Nitro-Carbazole Based Oxime Esters as Dual Photo/Thermal Initiators for 3D Printing and Composite Preparation. Macromolecular Rapid Communications, 2021, 2100207.

[18] Z. Li, X. Zou, G. Zhu, X. Liu, R. Liu, Coumarin-based oxime esters: photobleachable and versatile unimolecular initiators for acrylate and thiol-based click photopolymerization under visible light-emitting diode light irradiation. ACS applied materials & interfaces, 2018, 10.18: 16113-16123.

[19] W. Qiu, M. Li, Y. Yang, Z. Li, K. Dietliker, Cleavable coumarin-based oxime esters with terminal heterocyclic moieties: photobleachable initiators for deep photocuring under visible LED light irradiation. Polymer Chemistry, 2020, 11.7: 1356-1363.

[20] W. Qiu, J. Zhu, K. Dietliker, Z. Li, Polymerizable Oxime Esters: An Efficient Photoinitiator with Low Migration Ability for 3D Printing to Fabricate Luminescent Devices. ChemPhotoChem, 2020, 4.11: 5296-5303.

[21] J. Kirschner, J. Paillard, B. Graff, J.M. Becht, J.E. Klee, J. Lalevée, 2-Oxo-2(tert butyldimethylsilyl)Acetic Acid (DKSi-COOH) as a New Water-Soluble Visible Light Type I Photoinitiator for Free Radical Polymerization. Macromol. Chem. Physic, 2020, 221: 1900495.

[22] J. Lalevée, M.A. Tehfe, F. Dumur, D. Gigmes, N. Blanchard, F. Morlet-Savary, J.P. Fouassier, Iridium photocatalysts in free radical photopolymerization under visible lights. ACS Macro Lett, 2012, 1.2: 286–290.

[23] J. Lalevée, N. Blanchard, M. A. Tehfe, M. Peter, F. Morlet- Savary, D. Gigmes and J. P. Fouassier, Efficient Dual Radical/Cationic Photoinitiator under Visible Light: A New Concept, Polym. Chem., 2011, 2, 1986–1991.

[24] M. Abdallah, T. T. Bui, F. Goubard, D. Theodosopoulou, F. Dumur, A. Hijazi, J. P. Fouassier and J. Lalevée, Phenothiazine derivatives as photoredox catalysts for cationic and radical photosensitive resins for 3D printing technology and photocomposite synthesis. Polymer Chemistry, 2019, 10.45: 6145-6156.

[25] A. AL Mousawi, F. Dumur, P. Garra, J. Toufaily, T. Hamieh, F. Goubard, T.T. Bui, B. Graff, D. Gigmes, J.P. Fouassier, J. Lalevée, Azahelicenes as Visible Light Photoinitiators for

Cationic and Radical Polymerization: Preparation of Photoluminescent Polymers and Use in High Performance LED Projector 3D Printing Resins. J. Polym. Sci., 2017, Part A, 55: 1189–1199.

[26] E. Hola, J. Ortyl, M. Jankowska, M. Pilch, M. Galek, F. Morlet-Savary, B. Graff, C. Dietlin, J. Lalevée, New bimolecular photoinitiating systems based on terphenyl derivatives as highly efficient photosensitizers for 3D printing application. Polymer Chemistry, 2020, 11**:** 922–935.

[27] A.H. Bonardi, F. Dumur, D. Gigmes, Y.Y. Xu, J. Lalevée, Light-Induced Thermal Decomposition of Alkoxyamines upon Infrared CO2 Laser: Toward Spatially Controlled Polymerization of Methacrylates in Laser Write Experiments. ACS Omega, 2020, 5: 3043−3046.

[28] Y.Y. Xu, G. Noirbent, D. Brunel, Z. Ding, D. Gigmes, B. Graff, P. Xiao, F. Dumur, J. Lalevée, Novel ketone derivative-based photoinitiating systems for free radical polymerization under mild conditions and 3D printing. Polymer Chemistry, 2020, 11**:** 5767–5777.